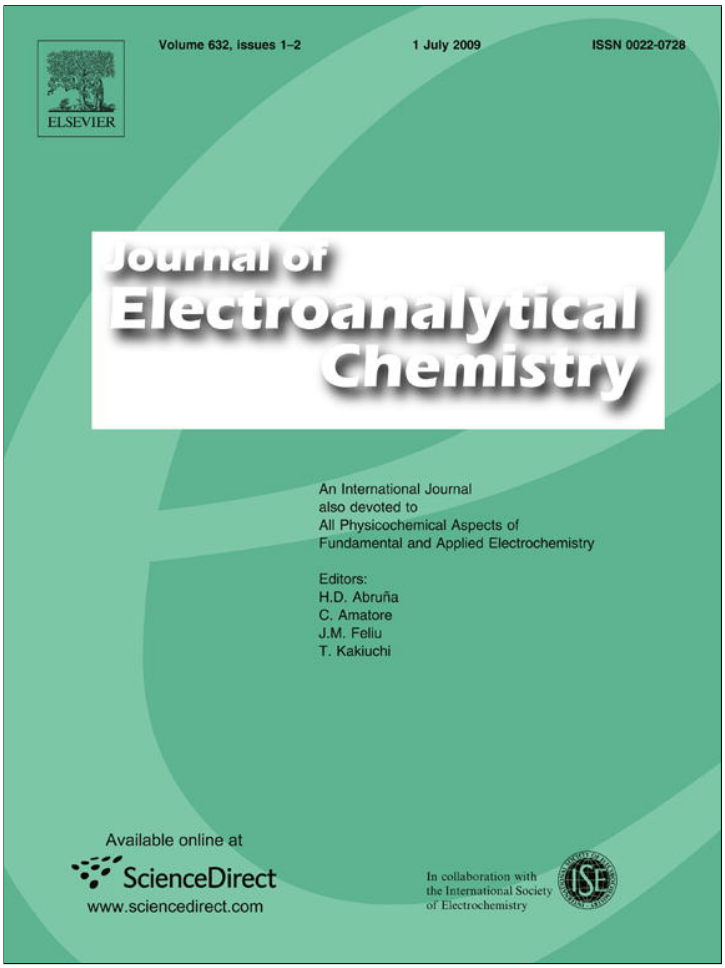

Journal of Electroanalytical Chemistry 632 (2009) 64–71

Contents lists available at ScienceDirect

Journal of Electroanalytical Chemistry

journal homepage: www.elsevier.com/locate/jelechem

Characterization of the anodic growth and dissolution of antimony oxide films

Omar E. Linarez Pérez, Manuel A. Pérez, Manuel López Teijelo *

INFIQC – Departamento de Fisicoquímica, Facultad de Ciencias Químicas, Universidad Nacional de Córdoba, Haya de la Torre y Medina Allende, 5000 Córdoba, Argentina

ARTICLE INFO

Article history:
Received 3 November 2008
Received in revised form 24 March 2009
Accepted 26 March 2009
Available online 5 April 2009

Keywords:
Antimony oxide
Oxide growth
Oxide dissolution
High-field growth
Ellipsometry

ABSTRACT

The anodic growth, morphology and stability of antimony oxide films grown in buffered phosphate electrolytes has been characterized by electrochemical methods, *in situ* ellipsometry and atomic force microscopy. The anodic voltammetric behaviour for the growth of antimony oxide films at low potentials can be interpreted as the stepwise electroformation of different antimony species with formation of soluble species up to give Sb_2O_3. This is followed by the anodic film growth at higher potentials through an ionic conduction mechanism caused by a 'high field', which drives the ionic migration as in typical "valve" metals. Ellipsometric results indicate that anodic films dissolve in the electrolysis media. Anodic Sb_2O_3 films are anisotropic, with complex refractive indices lower than those of crystalline antimony oxides. This is ascribed to hydration, anions incorporation or lack of crystalline structure in anodic oxides. The electric field strength obtained from the thickness/potential dependence, results 2.25×10^6 V cm^{-1}, which also supports that anodic Sb_2O_3 growth takes place by an ionic current driven by a high electric field within the oxide film. Morphology of anodic Sb_2O_3 films obtained by AFM shows that surfaces are smooth and flat and films are pore-free. The grain texture depends on concentration of electrolyte as a consequence of a different chemical dissolution rate. The stability of passive antimony oxide films at open circuit was analyzed by cyclic voltammetry with either constant or increasing anodic switching potentials. The overall growth and dissolution of antimony oxide films is described in terms of the oxide film growth by the high-field migration model coupled with a homogeneous dissolution process. The parameters A and β in the equation $i = A \exp(\beta\varepsilon)$ that characterize the dependence between current growth and field strength in the high-field growth as well as dissolution current for different conditions are obtained. Dissolution current dependence with electrolyte properties, indicate that antimony oxide dissolution is promoted by phosphate ions and is almost independent of pH.

1. Introduction

Due to the large diversity of properties, passive oxide films and their stability play an important role in present research [1]. The electrochemical behaviour of "valve" metals has been extensively studied due to their applications in optical films, microelectronics, capacitor manufacturing as well as corrosion protection [1,2].

Anodic oxidation of antimony has been comparatively less studied. The literature on the anodic behaviour of metallic Sb was mostly concerned with its use a pH indicator electrode [3]. More recently, antimony oxide (Sb_2O_3) has found many other applications as electrocatalyst and photoconductor, for thin film capacitors and in preparing electrochromic display devices.

The anodic growth of antimony oxide has been also the subject of research because antimony is used in lead alloys for lead-acid batteries. Most of the work on the electrochemical behaviour of Sb found in the literature has been performed in sulphuric acid solutions [4–10] although some studies in other acidic electrolytes such as phosphoric acid solutions, have been published [11,12].

Although antimony oxide is widely used, its durability is low due to corrosion and oxide dissolution processes. Pavlov et al. [5–7] have determined by electrochemical, XPD and SEM measurements that the corrosion process in sulphuric solutions takes place at open circuit as well as at low overpotentials. The passive layers formed in the early stages of oxidation consist of amorphous antimony oxide or hydroxide but at long oxidation times, aggregates or crystals are formed. The dissolution rate of the oxide films formed in sulphuric acid solutions was found to increase linearly with increasing acid concentration, while in phosphoric acid solutions it increases with pH of the electrolyte [13]. Mogoda et al. have studied the formation and currentless dissolution of antimony oxide films in H_2SO_4 solutions containing electroactive species like dichromate ions [14,15] or carboxylic acids (formic, acetic and propionic acids) as dissolution inhibitors [9]. More recently, Metikoš-Huković et al. [10] determined that the rate of antimony dissolution is promoted by addition of HSO_4^- ions as well as the increase in electrode rotation rate.

* Corresponding author. Tel.: +54 351 4334169; fax: +54 351 4334188.
E-mail address: mlopez@fcq.unc.edu.ar (M.López Teijelo).

0022-0728/$ - see front matter © 2009 Elsevier B.V. All rights reserved.
doi:10.1016/j.jelechem.2009.03.018

Although the kinetics of the anodic growth of antimony oxide has also been studied, no agreement on the mechanism of anodic oxide growth has been reached. Bojinov et al. [12] have reported that the anodic oxidation of antimony in H_3PO_4 solutions suggest the validity of the low-field approximation for anodic film growth. On the other hand, the impedance response of antimony and bismuth electrodes was explained using a kinetic model for the passivation of metals via formation of a dual layer comprising a barrier film and a salt overlayer, which is based on a high field-assisted migration of ions within the film [16].

This work reports on the study of the anodic growth, morphology and stability of antimony oxide films grown on antimony in buffered phosphate electrolytes by means of electrochemical methods, *in situ* ellipsometry and atomic force microscopy (AFM). In addition, kinetic parameters for oxide film growth assuming a high-field migration model as well as film dissolution rates are obtained.

2. Experimental

The working electrodes consisted of polycrystalline antimony rods (Goodfellow, 99.999% purity) of 6 mm diameter (0.28 cm^2 of geometric area) mounted in Teflon holders. A platinum sheet of 5 cm^2 was used as counter electrode. Potentials were measured versus the saturated calomel reference electrode (SCE). The surface of the antimony electrodes was pre-treated first with emery paper abrasion followed by mechanical polishing with 9, 3 and 1 μm diamond paste on a Nylon cloth and, finishing with 0.05 μm Al_2O_3 on Microcloth (Buehler). Measurements were performed at 25 °C in aqueous solutions prepared from AR chemicals and purified water (Milli Ro–Milli Q system). x M buffered phosphate solutions ($0.001 \leqslant x \leqslant 0.5$) in the pH range of 2–10 were employed as electrolyte. All solution used were deaerated by bubbling nitrogen before the oxide growth. Electrochemical measurements were carried out using a 173 EG&G PAR potentiostat/galvanostat coupled to a 175 EG&G PARC signal generator and a 7090A Hewlett Packard plotting recorder.

The anodic growth of the antimony oxide films was performed by direct anodic polarization of mechanically polished surfaces of antimony by applying triangular potential sweeps at different sweep rates either with constant or increasing anodic switching potentials.

To characterize the optical behaviour during the growth of anodic antimony oxide films as well as during dissolution at the open circuit potential, *in situ* ellipsometric measurements were performed during the electrochemical experiments. In some experiments, the anodic growth was performed galvanostatically. Optical measurements were performed using a Rudolph Research rotating-analyzer automatic ellipsometer (vertical type, 2000 FT model), equipped with a 75 W tungsten lamp as light source and a filter (546.1 nm). The *in situ* ellipsometric experiments were carried out using a three-compartment cell made of Pyrex glass. The working electrode was placed horizontally in the cell compartment, which has two plane glass windows adequate for optical measurements. The incidence angle used for all experiments was 70.00°. The light reflected by the electrode surface was passed through the rotating analyzer to a photomultiplier tube (PMT) for detection. The sinusoidal output of the PMT was digitized by a HP microcomputer and the values of the ellipsometric angles Ψ and Δ were calculated by the computer from the three Fourier coefficients of the PMT signal. The PMT signal was averaged twice and data were collected in continuous mode. The time interval between measurements was *ca.* 1 s.

During the growth of thick films, the ellipticity angle, ε, (as defined in Ref. [17], p. 8), changes in sign ($-\pi/4 \leqslant \varepsilon \leqslant \pi/4$) during the experiment. In a rotating-analyzer ellipsometer, the sign of the ellipticity must be entered before starting the measurement [18]. Therefore, it is necessary to stop the measurement in the region of change of sign, change the sign in the equipment and then restart the measurement. This defines two loops in the Ψ–Δ plane, which correspond to $0 \leqslant \Delta \leqslant 180°$ and to $180° \leqslant \Delta \leqslant 360°$.

The optical data were fitted by employing either an isotropic or an anisotropic single-layer model. In both cases, it is assumed that oxide film growth takes place as a single layer (isotropic or anisotropic) of constant optical properties that grows on a flat bare antimony substrate. The fitting model uses the Simplex method [19] to minimize the error function:

$$G = \frac{1}{m}\sum_i \left[(\Delta_i^{\exp} - \Delta_i^{calc})^2 + (\Psi_i^{\exp} - \Psi_i^{calc})^2\right]^{1/2} \quad (1)$$

where the superscript "*calc*" denotes the values calculated from the model. No assumptions on the values of the optical properties of the oxide were made in fitting the experimental response, allowing the Simplex algorithm to vary the refractive index (n) and the extinction coefficient (k) for the isotropic film or the corresponding values in the normal (or ordinary; $\boldsymbol{n_{ord}} = n_{ord} - k_{ord}i$) and parallel (or extraordinary; $\boldsymbol{n_{extr}} = n_{extr} - k_{extr}i$) directions to the surface for the anisotropic layer. Film thickness is an additional parameter that is also optimized in the fitting process and once the optical response is fitted in terms of a given model, both the optical properties and thickness of the oxide films are obtained.

AFM measurements were performed in air in contact mode at room temperature using a PicoScan SPM Molecular Imaging Microscope and triangular silicon probes coated with a W/Al film (0.35 N m^{-1}).

Simulation of the *j*/*E* potentiodynamic profiles for the oxide growth were performed by integration of the corresponding differential equations using the Runge-Kutta (fourth order) algorithm written in FORTRAN [19], employing the boundary conditions given in Ref. [2], p. 250, as described previously in Ref. [20]. The potentiodynamic response was simulated for repetitive potential sweeps for increasing anodic switching potentials, for given values of the kinetic parameters and physical properties of the antimony oxide. In order to obtain the dissolution current values, data were fitted employing non-linear least square routines (Table Curve software from Jandel Scientific) according to the procedure previously described [20].

3. Results and discussion

3.1. General electrochemical behaviour

Fig. 1 shows the potentiodynamic *j*/*E* response obtained at 0.1 V s^{-1} of a mechanically polished antimony electrode in a 0.1 M $NaH_2PO_4 + Na_2HPO_4$ (pH 7) solution by applying triangular potential sweeps (see inset in Fig. 1) between the potential limits corresponding to the hydrogen and oxygen evolution reactions. During the positive scan the current profile shows two main anodic peaks between −0.2 and +0.9 V (potential zone I) and, afterwards, it reaches a steady-state value that remains constant up to *ca.* 3.5 V (zone II). At more positive potentials, anodic current increases again, defining a second nearly constant current region of potential (zone III), which is poorly reproducible, before reaching the oxygen evolution (zone IV).

The anodic peaks at low potentials (zone I), which correspond to the potential range of antimony active dissolution, have been attributed to the metal electro-oxidation to trivalent antimony species through a three-stage reaction mechanism that includes the formation of oxygen-containing species ($Sb(OH)_{ad}$; $Sb(O)_{ad}$) as well as SbO^+ soluble species [5,6]. As concentration of antimony

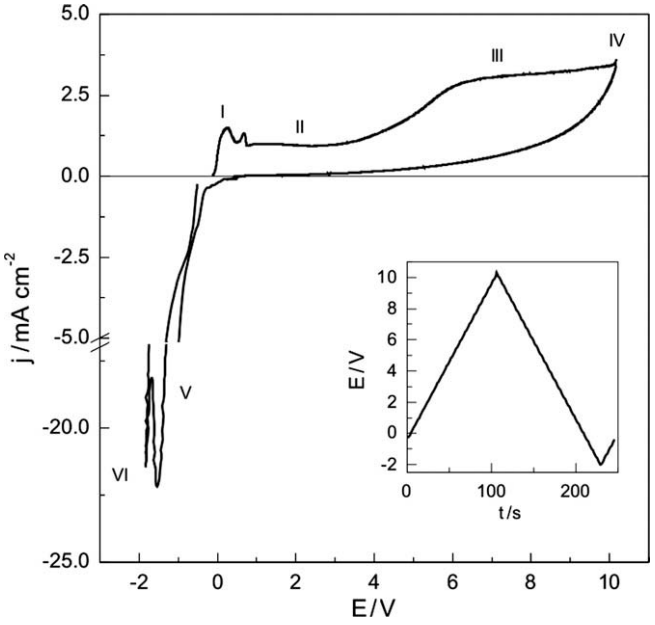

Fig. 1. Potentiodynamic j/E response at 0.1 V s^{-1} of a mechanically polished antimony electrode applying a triangular potential sweep (see program) in a 0.1 M [NaH_2PO_4 + Na_2HPO_4] (pH = 7) solution.

surface species increases, an anodic oxide layer of Sb_2O_3 can be formed leading to passivation of the surface. The physical and conduction properties of the oxide layer determine, in turn, the kinetics and mechanism and of growth. Once a given thickness of Sb_2O_3 is established, kinetics of growth change and the steady-state current, j_{ss}, obtained in the 0.9–3.5 V potential range (zone II) is attributed to the anodic growth of the Sb_2O_3 film, according to the overall reaction:

$$2Sb(s) + 3H_2O \rightarrow Sb_2O_3(s) + 6H^+(aq) + 6e^- \quad (2)$$

assuming that the contribution of other processes like capacitive charging or chemical dissolution is negligible. Under these conditions, the total current corresponds to the ionic current and the charge passed makes the oxide film thicker and, consequently, the steady-state current corresponds to a constant growth rate. This j/E response in zone II corresponds to that exhibited by the so-called "valve" metals, where the oxide growth takes place through an ionic conduction mechanism caused by a 'high field' [2]. For metals that show this behaviour, it is accepted that the potential drop takes place entirely across the oxide film that generates a high electric field, which drives the ionic migration [2,20]. Since the ionic current only depends on the electric field (see Eq. (3) below), a steady-state current also indicates that the electric field remains constant during the oxide growth under given experimental conditions. j_{ss} increases almost linearly with potential scan rate, according to expected for anodic growth through a "high-field mechanism" and commonly found for oxide growth on other valve metals as tungsten [21]. At higher potentials (zone III) anodic growth continues, probably following the same oxide growth mechanism. Nevertheless, the oxygen evolution contribution that would take place well-before the massive oxygen evolution (zone IV), prevents a quantitative evaluation of growth rate in potential zone III from potentiodynamic experiments only.

The reversal of the potential scan produces a decrease of the anodic current due to the decrease of the electric field. The current remains low within a wide range of potentials, indicating that no noticeable anodic processes are observed on the electrode after the anodic oxide film has been formed. For potential values lower than −0.2 V, the cathodic current peak obtained (zone V) is associated with the electroreduction of the Sb_2O_3 film electroformed during the positive scan [5,6]. At potentials more negative than −1.65 V (zone VI), the hydrogen evolution reaction on the antimony electroreduced surface takes place.

Fig. 2 shows the potentiodynamic j/E response of polished antimony surfaces obtained in 0.1 M NaH_2PO_4 + Na_2HPO_4 solutions of different pH. The anodic current response in the −0.2 V to +0.9 V range is modified slightly with pH changes since formation of different soluble species is involved in this potential region [5,6]. On the contrary, in the potential range corresponding to zone II for anodic Sb_2O_3 film growth, the current profile is practically independent of pH indicating that anodic oxide growth rate is not dependent on acidity. This result is consistent with the assumption that in zone II the anodic growth takes place through an ionic migration within the film, according to the "high-field" mechanism.

3.2. Ellipsometric results

In order to gain a deeper insight on the anodic oxide growth process as well as on the oxide stability at open circuit, the ellipsometric response during potentiodynamic growth and after opening the circuit was obtained. Fig. 3 shows the variation of the ellipsometric angles Ψ and Δ during the potentiodynamic polarization a 0.1 V s^{-1} of a mechanically polished antimony surface in a 0.1 M NaH_2PO_4 + Na_2HPO_4 (pH 7) solution. The corresponding j/E response is also shown for comparison. Starting from the Ψ and Δ values corresponding to the freshly polished antimony substrate (covered by a thin spontaneous oxide layer), in the −0.2 V to +0.9 V potential range the optical response defines a small loop in the Ψ–Δ plane, which can be associated with growth of a film with a low refractive index (n_f) value. This would correspond to the anodic formation of a highly hydrated oxide film [22] in the potential zone I. At potentials higher than 1.0 V, the Ψ–Δ response (open symbols) shows the typical changes associated with the growth of a film on a valve metal [23–26], and presents the most important changes in the values of Ψ and Δ. At potentials exceeding around 4.5 V, the changes follow the same tendency but are less important and the Ψ and Δ values show some increasing scattering making the optical response poorly reproducible in this potential range. The detailed analysis of the ellipsometric response in potentiodynamic experiments will be given in a forthcoming paper [27]. During the negative sweep (open squares) the ellipsometric angles remain almost constant indicating that oxide growth practically stops.

Fig. 3 also shows the Ψ and Δ values obtained after opening the circuit (dashed line). It can be seen that initially the optical response during dissolution practically retraces the response ob-

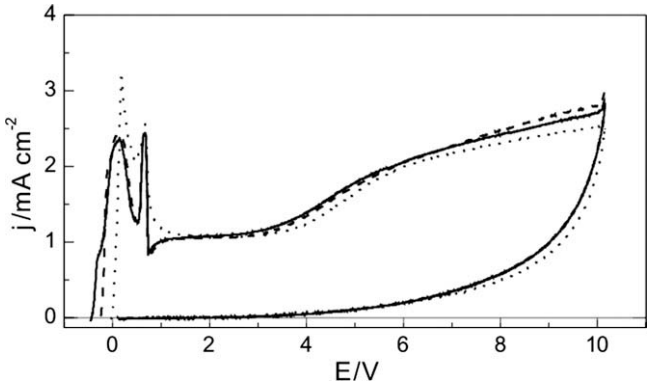

Fig. 2. Potentiodynamic j/E response at 0.1 V s^{-1} of a mechanically polished antimony electrode in 0.1 M [NaH_2PO_4 + Na_2HPO_4] solutions of pH: 2 (· · · ·), 7 (- - - -) and 10 (——).

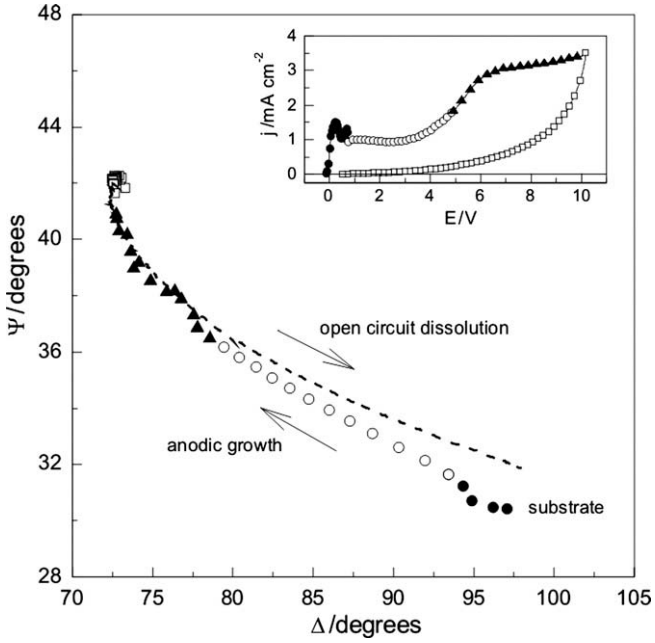

Fig. 3. Ψ–Δ response during the potentiodynamic growth of a Sb_2O_3 film up to *ca.* 10 V (υ = 0.1 V s^{-1}) on a mechanically polished antimony surface and the subsequent circuit opening. 0.1 M [NaH_2PO_4 + Na_2HPO_4] (pH = 7).

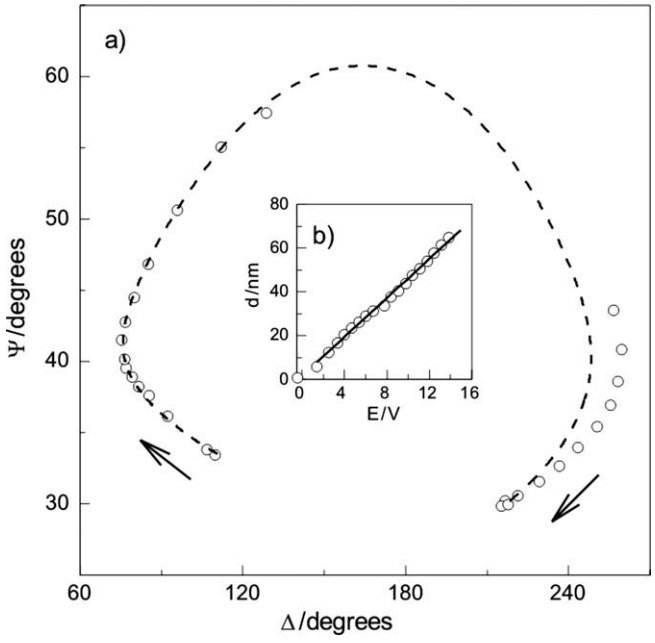

Fig. 4. Ψ–Δ response during the galvanostatic growth of a Sb_2O_3 film up to *ca.* 60 V (j = 2.86 mA cm^{-2}) on a mechanically polished antimony surface. 0.1 M [NaH_2PO_4 + Na_2HPO_4] (pH = 7).

tained during oxide growth but then shows a progressive departure. After around 20 min, Ψ and Δ reach values that are near those corresponding to the polished substrate, indicating that oxide film is completely dissolved. The difference of Ψ and Δ values corresponding to the substrate before the oxide growth and after film dissolution indicates that the optical properties of the surface are affected by the chemical dissolution process, mainly as a consequence of surface roughness generation [23]. In summary, these results together with those of the previous section are interpreted as the electroformation of a hydrated film involving different antimony species up to finally yield the Sb_2O_3 oxide that grows following a high-field mechanism. The Sb_2O_3 layer dissolves chemically in the electrolysis media giving soluble SbO^+ species.

Under potentiodynamic conditions, massive oxygen evolution taking place at potentials higher than *ca.* 10 V (not shown) limits the oxide growth process (thickness values not higher than around 40 nm are obtained; see below). Due to this, in order to study the oxide growth in a wider range of thickness ($0 < d < 150$ nm) the Sb_2O_3 films were grown under galvanostatic conditions [23,24]. Fig. 4a shows the Ψ–Δ response obtained during the galvanostatic growth (j = 2.86 mA cm^{-2}) of a Sb_2O_3 film up to a final thickness of around 150 nm ($E_f \approx 30$ V). The data corresponding to the first loop ($\Delta < 180°$) can be reasonably fitted with the anisotropic single-layer model with small error values (dotted line), which allows obtaining reliable values for the optical properties of the film as well as thickness at the different stages of growth. At high thickness (or potential) values (second loop; $\Delta > 180°$), the Ψ–Δ response deviates from that predicted by the simulation employing optical properties obtained in the first loop. This can be attributed to changes in the optical properties during growth since at long times other processes (such as roughening and ageing) may become of importance [23,24]. Under the anodizing conditions employed, the ordinary and extraordinary complex refractive indices ($\boldsymbol{n} = n - ki$) obtained, are $\boldsymbol{n_{ord}} = 1.954 - 0.002i$, $\boldsymbol{n_{extr}} = 1.985 - 0.042i$, indicating that the anodic Sb_2O_3 films are anisotropic. The values obtained for the refractive indices of the anodic film, n_f, are lower than those reported for *valentinite*, a natural Sb_2O_3 that crystallizes in the orthorhombic system, which is also an anisotropic material (n_α = 2.18; $n_\beta = n_\gamma$ = 2.35) [28]. Another natural Sb_2O_3, *sénarmontite*, which presents a cubic structure, is isotropic (n = 2.087) [28]. The lower values obtained for the refractive indices of anodic oxides as compared with known crystalline oxides could be attributed to hydration, anions incorporation or lack of crystalline structure [22]. On the other hand, the low values obtained for the extinction coefficients ($k \approx 0$) indicate that the films are practically transparent, as found for other oxides formed on "valve" metals [23–25,29–32].

The thickness values, d, obtained from the fitting procedure show a linear dependence with the formation potential, E_f, (Fig. 4b). Assuming that the potential drop occurs within the film (i.e. potential drop at the interfaces is negligible), the calculated value for the electric field strength within the oxide film, ε, under the anodizing conditions employed (j = 2.86 mA cm^{-2}) results 2.25×10^6 V cm^{-1}, which is of the same order of magnitude as those obtained for other "valve" metals [1,33–35]. These results support that Sb_2O_3 growth takes place by an ionic current driven by the high electric field set up across the oxide film ("high-field" mechanism) [2].

3.3. AFM characterization

Morphology of anodic Sb_2O_3 films grown at different electrolyte concentrations was obtained by AFM experiments. Films were prepared by applying a linear potential sweep up to 3 V, then she surface was washed with purified water, dried at room temperature under nitrogen and the AFM images were acquired in air. Fig. 5 shows 3D AFM images obtained from the anodized antimony surface at two different phosphate concentrations. Surface morphology shows that films are pore-free and that the texture obtained is dependent on formation electrolyte concentration. Nevertheless, the *rms* values obtained in both cases are very similar (note that the horizontal extent of the AFM scans is 20 times greater than the vertical scale, meaning that the surface features are greatly over-emphasized and, hence, the surfaces are actually very smooth and flat). Furthermore, the roughness factor, r, defined as the ratio between the area of the topography and the nominal or geometri-

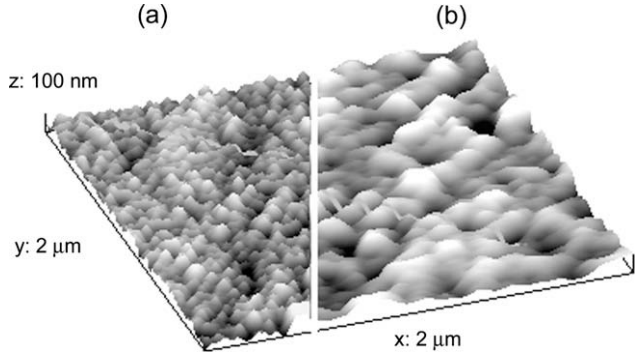

Fig. 5. AFM 3D images of a 2 μm × 2 μm area obtained after the potentiodynamic growth at 0.05 V s^{-1} up to a final potential of 3 V, of a Sb_2O_3 film on a mechanically polished antimony surface in (a) 0.1 M and (b) 0.002 M [NaH_2PO_4 + Na_2HPO_4] solutions (pH 7).

cally projected area of topography, are also very similar, resulting values of 1.03 ± 0.02 and 1.01 ± 0.02 for films formed in phosphate 0.002 M and 0.1 M, respectively. The *r* values have been calculated as described in Ref. [36], employing the software reported in Ref. [37]. The absolute values of *r* should be taken judiciously, as acquisition and treatment of the surface topography data influence their calculated values. The values obtained for images taken under the same conditions except the electrolyte concentration, are only informed for comparison.

In summary, from the analysis of the surface morphology, it can be concluded that anodic Sb_2O_3 films formed in phosphate solutions are pore-free and that the different textures obtained are a consequence of a different chemical dissolution rate as electrolyte concentration is changed (see below). Furthermore, obtaining smooth surfaces is consistent with the anodic growth mechanism ("high-field mechanism") as well as with a homogeneous dissolution rate or chemical dissolution process.

3.4. Oxide film stability

The open circuit stability of passive oxide films has been investigated by potentiodynamic reformation experiments [38] or cyclic polarization measurements [34,39], capacitance measurements [40,41] and ellipsometry [23,24,42], among others. Notwithstanding, the use of cyclic voltammetry either with constant or increasing anodic switching potentials is by far much more simple in order to characterize the anodic oxide growth and dissolution on valve metals for a given system under determined experimental conditions.

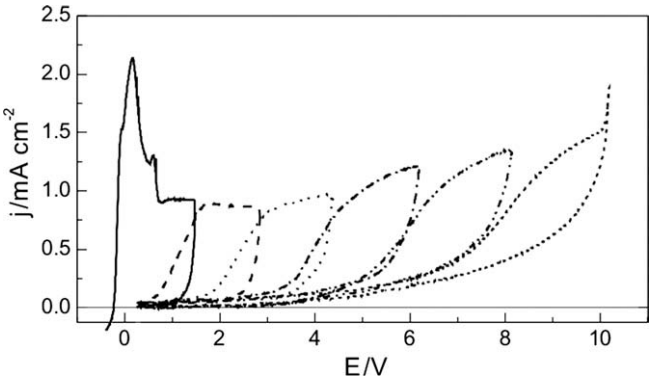

Fig. 6. Potentiodynamic *j*/*E* response at 0.1 V s^{-1} of a mechanically polished antimony electrode by applying repetitive potential sweeps with increasing anodic switching potentials in a 0.1 M [NaH_2PO_4 + Na_2HPO_4] solution (pH 7).

Fig. 6 shows the potentiodynamic *j*/*E* response obtained at 0.1 V s^{-1} for a polished antimony electrode in a 0.1 M [NaH_2PO_4 + Na_2HPO_4] solution (pH 7) by applying repetitive triangular potential sweeps with increasingly anodic switching potentials. After the anodic peaks obtained in the −0.2 V to +0.9 V potential range attributed to the stepwise formation of different antimony oxygen-containing species up to give Sb_2O_3, the steady-state current corresponding to the anodic growth by "high field" is obtained. During the second cycle, current starts to increase at low potentials indicating that some part of the Sb_2O_3 film has been lost as a consequence of chemical dissolution. This is clearly seen in successive cycles, where an important curve-crossing between successive cycles due to the increasing importance of chemical dissolution of the oxide film as time increases, is noticed. This behaviour together with the topographic information obtained by AFM, are interpreted as a homogeneous chemical dissolution process coupled to the anodic oxide growth.

Recently, we have reported the methodology for obtaining quantitative information on the parameters characterizing the high-field oxide growth as well as the oxide dissolution rate on valve metals assuming that growth takes place by high-field transport of ions within the oxide film [20]. When valve metals are anodically polarized, oxide films grow irreversibly by a field-assisted migration of ions through the film following the so-called "high-field" model [2]. Neglecting electron transfer contributions or capacitive charging, the ionic growth current density, j_{ox}, (transfer of oxygen ions from the electrolyte into the oxide) is given by

$$j_{ox} = A\exp(\beta\varepsilon) \tag{3}$$

where $\varepsilon = \eta/d$ is the electric field strength, η is the overpotential for the metal oxidation process, d the oxide film thickness and A and β are temperature-dependent parameters characteristic of the oxide [2]. The microscopic interpretation of the parameters A and β, which is based on the theory of ionic transport through solids has been given previously [2] but for the purposes of the present work A and β can be considered as temperature-dependent macroscopic parameters that characterize the kinetics of growth ("high-field" growth; Eq. (3)). If the potential drop at the interfaces is negligible and in the absence of space charge effects, the electric field is obtained from the overpotential for the metal oxidation process and the oxide film thickness, d, which depends on time as well as the existence of a dissolution current, j_d, due to chemical dissolution of the oxide. From solution of Eq. (3) under potentiodynamic conditions [2,20] the following relationship, which gives the current/time (or current/potential) dependence, is obtained:

$$\frac{dy}{dt} = \frac{1}{t}y\ln(y)\left\{1 - \left[\frac{MA}{nF\delta_{ox}\beta\upsilon}\left(y - \frac{1}{A}j_d\right)\ln(y)\right]\right\} \tag{4}$$

where $y = j_{ox}/A$, υ is the potential scan rate, δ_{ox} the oxide density, M the oxide molecular weight, n the number of electrons exchanged and F the Faraday constant.

The application of a linear potential sweep establishes a steady-state current value, j_{ss}, after the initial increase of current, which is typical for oxide growth on valve metals. The rearranged expression obtained for j_{ss}, (equating Eq. (4) to zero), is:

$$\ln(j_{ss}) = \ln(A) + \left(\frac{nF\delta_{ox}\beta}{M}\right)\left[\frac{\upsilon}{j_{ss} - j_d}\right] \tag{5}$$

which gives the relationship between j_{ss} and υ for given values of the parameters A, β and j_{ss}, besides the physical properties of the oxide [20]. The dependence of j_{ss} with υ employing a potentiodynamic perturbation provides all the information needed for obtaining the parameters A and β as well as j_d for a given system. In the absence of chemical dissolution, the usual practice is obtaining the values of A and β from the linear dependence $\ln(j_{ss})$ vs. (υ/j_{ss}) (this limit is obtained from Eq. (5) for $j_d = 0$), provided that the phys-

ical constants of the oxide are known [43,44]. On the other hand, in the presence of a chemical dissolution process, Eq. (5) predicts a deviation from linearity as j_d becomes more important in relation to j_{ss}, i.e. at low scan rates.

In order to gain further insight on the chemical dissolution processes, the dependence of j_{ss} values (in the 1–3.5 V potential range, zone II) on scan rate during growth of antimony oxide under different experimental conditions, was obtained. Fig. 7 shows the ln (j_{ss}) vs. (υ/j_{ss}) plots for growth of antimony oxide in phosphate solutions of different concentration at pH 2 and 7. As can be clearly seen, increasing deviations are obtained at low scan rates as phosphate concentration increases. From the non-linear least square fit procedure employing Eq. (5), all the parameters (A, β and j_d) in zone II for the different conditions were obtained. The value of β was constant, resulting an average value of $\beta = (2.8 \pm 0.1) \times 10^{-6}$ cm V^{-1}. The value of A increased slightly with pH, resulting (0.36 ± 0.06) μA cm^{-2} and (0.58 ± 0.08) μA cm^{-2} for pH 2 and 7, respectively. These values are within those expected for anodic growth under "high-field" conditions, resulting similar to those reported in the literature for other "valve" metals [1,40,45,46]. The little variation in the A and β values would indicate that the growth kinetics is not modified substantially with the change in experimental conditions. Dissolution current values obtained from the fitting procedure change with the total anionic phosphate concentration, C_A, and pH, as expected. Fig. 8 shows log j_d vs. log C_A plots for the dissolution of anodic Sb_2O_3 films in phosphate electrolytes at different pH values. The log j_d vs. log C_A dependence is linear with a slope $\alpha = 1$, indicating that phosphate ions promote the dissolution process. On the other hand, dissolution rates are almost independent of pH. The specific constant rate, k_d, defined as $k_d = j_d/C_A$, decreases slightly with pH (inset in Fig. 8) with an average slope of around −0.05, indicating some participation of proton ions in the dissolution mechanism. Usually, oxides/hydroxides dissolution in aqueous solutions involves steps corresponding to H^+ (or OH^-) ions adsorption, i.e. surface processes at the oxide/electrolyte interface. Consequently, H^+ surface concentration is related to the bulk pH in a complex manner, which depends on the dissolution mechanism as well as the adsorption equilibrium steps, giving rise to overall fractional reaction orders

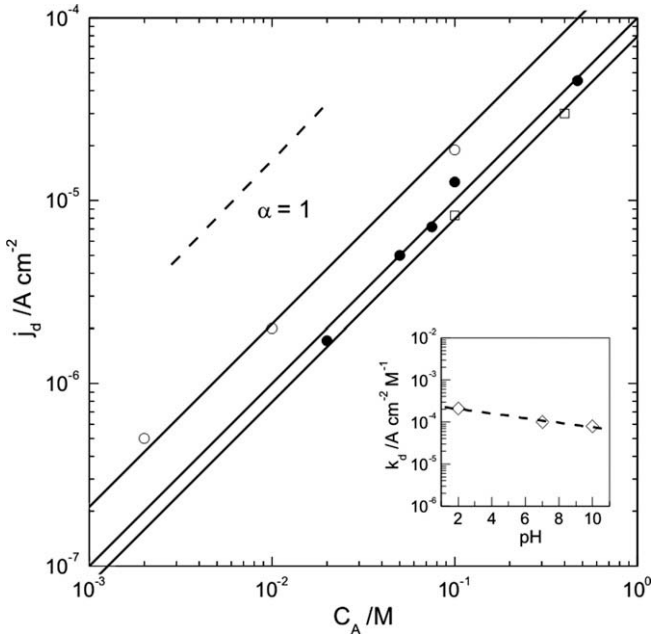

Fig. 8. Dependence of j_d values obtained from fitting (Fig. 7) on C_A at different pH values. Inset: dependence of k_d values on pH.

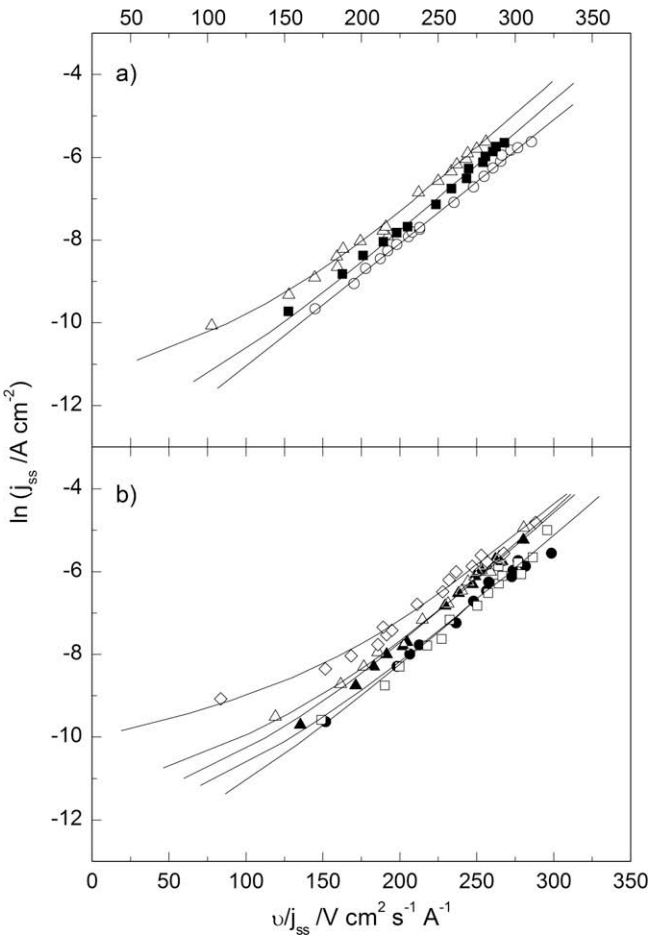

Fig. 7. Plots for ln (j_{ss}) vs. υ/j_{ss} for the anodic growth of Sb_2O_3 in x M buffered phosphate solutions of pH 2 (a) and 7 (b). x: 0.002 (○), 0.01 (■), 0.02 (●), 0.05 (□), 0.075 (▲), 0.1 (Δ) and 0.47 (◇). Full lines show best fit with Eq. (5).

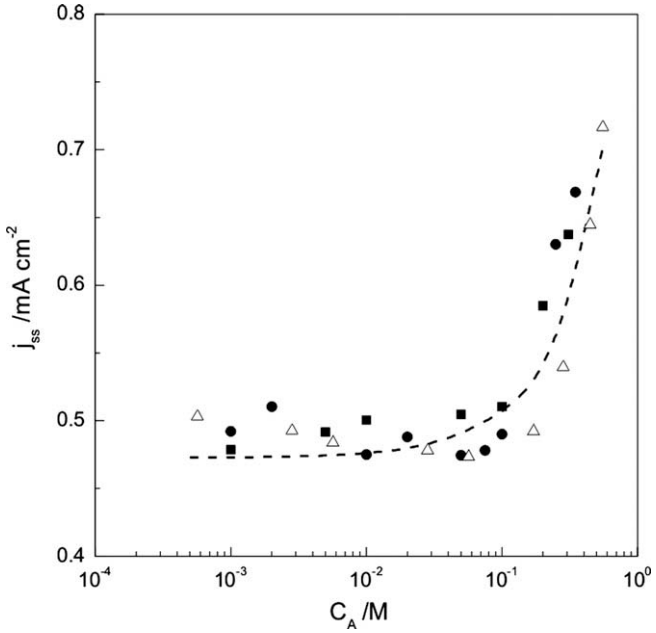

Fig. 9. Dependence of j_{ss} on C_A for the potentiodynamic growth at 0.1 V s^{-1} of Sb_2O_3 films in buffered phosphate solutions of pH 2 (Δ), 7 (●) and 10 (■). Dashed line shows the calculated dependence employing Eq. (5) (see text).

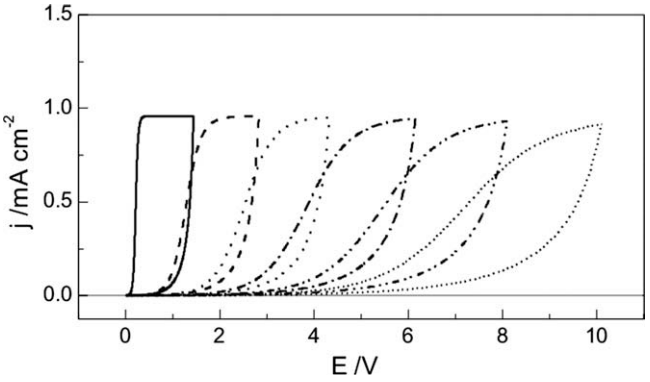

Fig. 10. Simulated potentiodynamic j/E response for the anodic growth of Sb_2O_3 by applying repetitive potential sweeps with increasing anodic switching potential based on the high-field conduction model with chemical oxide dissolution (Eq. (3)). Simulation parameters: $A = 0.54\ \mu A\ cm^{-2}$, $\beta = 2.8 \times 10^{-6}\ cm\ V^{-1}$, $n = 6$, $M = 291.5\ g\ mol^{-1}$, $\delta = 5.67\ g\ cm^{-3}$, $d_o = 2\ nm$, $j_d = 15\ \mu A\ cm^{-2}$, $\upsilon = 0.1\ V\ s^{-1}$.

even though the rate law in terms of the appropriate expression for the surface species concentration has an integer reaction order [47–50]. As an example, for the H^+-promoted dissolution of $Ni(OH)_2$ in different media, an average reaction order of around 0.35 is found for bulk protons concentration [50]. In summary, dissolution rate is promoted by phosphate ions (reaction order around 1) being almost independent of pH, although the analysis of a detailed mechanism for Sb_2O_3 film dissolution is out of the scope of this work.

In order to show the consistency of the analysis performed, Fig. 9 shows the variation of the steady-state current density, j_{ss}, obtained at $0.1\ V\ s^{-1}$ as a function of C_A for the different pH values employed, together with a calculation employing Eq. (5) and the values of j_d obtained from fitting for different concentrations. The good agreement between data and calculated curve indicates that the model employed, given by Eq. (5), describes properly the overall potentiodynamic behaviour of the system.

Additionally, the experimental results can also be compared with simulations employing the equations derived in Ref. [20]. Fig. 10 shows the simulated voltammogram for repetitive scans with increasing anodic switching potentials employing the values of the parameters obtained from the fitting procedure employed in Fig. 7, which clearly shows the curve-crossing in successive cycles similar to those obtained experimentally (see Fig. 6).

4. Conclusions

The voltammetric and ellipsometric results for the anodic growth of antimony oxide films grown in buffered phosphate electrolytes indicate that the anodic behaviour can be interpreted as the stepwise electroformation of different antimony species with formation of soluble species up to give Sb_2O_3, followed by the anodic film growth through an ionic conduction mechanism caused by a 'high field' which drives the ionic migration as in typical "valve" metals. Ellipsometric results also indicate that anodic films dissolve in the electrolysis media. The fitting of the ellipsometric response during growth indicates that anodic Sb_2O_3 films are anisotropic, with complex refractive indices lower than those of crystalline antimony oxides. This is attributed to hydration, anions incorporation or lack of crystalline structure in anodic oxides. From the dependence of thickness with potential and assuming that the potential drop takes place entirely across the oxide film, a value of $2.25 \times 10^6\ V\ cm^{-1}$ for the electric field strength is obtained. This value also supports the conclusion that anodic Sb_2O_3 growth takes place by an ionic current driven by a high electric field within the oxide film.

Morphology of anodic Sb_2O_3 films obtained by AFM shows that surfaces are smooth and flat and films are pore-free. The grain texture depends on concentration of electrolyte as a consequence of a different chemical dissolution rate.

The open circuit stability of passive oxide films, analyzed by cyclic voltammetry with either constant or increasing anodic switching potentials, provides quantitative information on the parameters characterizing the high-field oxide growth as well as the oxide dissolution rate on valve metals. Antimony oxide films stability is described in terms of the oxide film growth by a high-field migration model coupled with a homogeneous dissolution process. The comparison of experimental results with simulations is also consistent with this model.

From the dependence of the steady-state current for growth with scan rate in potentiodynamic experiments, the parameters A and β that characterize the high-field growth as well as dissolution current for different conditions are obtained. Values obtained for the parameters A and β are typical for the anodic growth on valve metals under "high-field" conditions. From the dependence of the dissolution current with experimental conditions, it is concluded that antimony oxide dissolution is promoted by phosphate ions being almost independent of pH.

Acknowledgements

Financial support from the Consejo Nacional de Investigaciones Científicas y Técnicas of Argentina (CONICET), the Agencia Nacional de Promoción Científica y Tecnológica (ANPCYT), and the Secretaría de Ciencia y Tecnología (SECYT-UNC) is gratefully acknowledged. OELP thanks CONICET for the fellowships granted.

References

[1] J.W. Schultze, M.M. Lohrengel, Electrochim. Acta 45 (2000) 2499.
[2] M.J. Dignam, in: J.O'M. Bockris, B.E. Conway, E. Yeager, R.E. White (Eds.), Comprehensive Treatise of Electrochemistry, vol. 4, Plenum, Publishing Corp., New York, 1981, p. 247. Chapter 5.
[3] V. Past, in: A.J. Bard (Ed.), Encyclopedia of Electrochemistry of the Elements, vol. 4, New York, 1975.
[4] M. Metikoš-Huković, B. Lovreček, Electrochim. Acta 25 (1980) 717.
[5] D. Pavlov, M. Bojinov, T. Laitinen, G. Sundholm, Electrochim. Acta 36 (1991) 2081.
[6] D. Pavlov, M. Bojinov, T. Laitinen, G. Sundholm, Electrochim. Acta 36 (1991) 2087.
[7] T. Laitinen, H. Revitzer, G. Sundholm, J.K. Vilhunen, D. Pavlov, M. Bojinov, Electrochim. Acta 36 (1991) 2093.
[8] M. Bojinov, I. Kanazirsky, A. Girginov, Electrochim. Acta 41 (1996) 2697.
[9] A.S. Mogoda, T.M. Abd El-Haleem, Thin Solid Films 441 (2003) 6.
[10] M. Metikoš-Huković, R. Babić, S. Brinić, J. Power Sources 157 (2006) 563.
[11] M.M. Hefny, W.A. Badawy, A.S. Mogoda, M.S. El-Basiouny, Electrochim. Acta 30 (1985) 1017.
[12] M. Bojinov, I. Kanazirski, A. Girginov, Electrochim. Acta 40 (1995) 873.
[13] M.M. Hefny, W.A. Badaway, A.S. Mogoda, M.S. El-Basiouny, Electrochim. Acta 30 (1985) 1017.
[14] A.S. Mogoda, Thin Solid Films 394 (2001) 174.
[15] A.S. Mogoda, T.M. Abd El-Haleem, Corrosion 59 (2003) 3.
[16] M. Bojinov, I. Kanazirsky, A. Girginov, Electrochim. Acta 41 (1996) 2695.
[17] R.M. Azzam, N.M. Bashara, Ellipsometry and Polarized Light, North Holland, Amsterdam, 1977.
[18] Manual for the automatic 2000FT ellipsometer (Rudolph Research).
[19] W.H. Press, B.P. Flannery, S.A. Teukolsy, W.T. Vetterling, Numerical Recipes: The Art of Scientific Computing, Cambridge, Cambridge, 1986.
[20] O.E. Linarez Pérez, V.C. Fuertes, M.A. Pérez, M. López Teijelo, Electrochem. Commun. 10 (2008) 433.
[21] M. Metikoš-Huković, Z. Grubač, J. Electroanal. Chem. 556 (2003) 167.
[22] S. Gottesfeld, in: A.J. Bard (Ed.), Electroanalytical Chemistry, vol. 15, Marcel Dekker, New York, 1989, p. 143.
[23] M.A. Pérez, M. López Teijelo, Thin Solid Films 449 (2004) 138.
[24] M.A. Pérez, M. López Teijelo, J. Phys. Chem. B 109 (2005) 19369.
[25] M.A. Pérez, M. López Teijelo, J. Electroanal. Chem. 583 (2005) 212.
[26] M.A. Pérez, O.E. Linarez Pérez, M. López Teijelo, J. Electroanal. Chem. 596 (2006) 149.
[27] O.E. Linarez Pérez, M.D. Sánchez, M. López Teijelo, in preparation.
[28] D.R. Lide (Ed.), Handbook of Chemistry and Physics, 73rd ed., (1992–1993), CRC Press, Boca Raton.
[29] J.L. Ord, P. Wang, J. Electrochem. Soc. 130 (1983) 1809.
[30] E.M. Patrito, V.A. Macagno, J. Electrochem. Soc. 140 (1993) 1576.
[31] J.C. Clayton, D.J. De Smet, J. Electrochem. Soc. 123 (1976) 174.

[32] D.J. De Smet, J.L. Ord, J. Electrochem. Soc. 130 (1983) 280.
[33] E.M. Patrito, R.M. Torresi, E.P.M. Leiva, V.A. Macagno, J. Electrochem. Soc. 137 (1990) 524.
[34] H. Lee, F. Xu, C.S. Jeffcoate, H.S. Isaacs, Electrochem. Solid-State Lett. 4 (2001) B31.
[35] O.E. Linarez Pérez, V.C. Fuertes, M.A. Pérez, M. López Teijelo, in: Proceedings of the Symposium on Corrosion, PV 2001-22, The Electrochemical Society, 2001, pp. 99–106.
[36] P.J. Ramón-Toregrosa, M.A. Rodríguez-Valverde, A. Amirfazli, M.A. Cabrerizo-Vilchez, Colloids Surf. A: Physicochem. Eng. Asp. 323 (2008) 83–93.
[37] I. Horcas, R. Fernández, J.M. Gómez-Rodríguez, J. Colchero, J. Gómez-Herrero, A.M. Baró, Rev. Sci. Instrum. 78 (2007) 013705.
[38] D.J. Blackwood, L.M. Peter, D.E. Williams, Electrochim. Acta 33 (1988) 1143.
[39] C.J. Boxley, J.J. Watkins, H.S. White, Electrochem. Solid-State Lett. 6 (2003) B38.
[40] M.M. Hefny, A.G. Gadalla, A.S. Mogoda, Bull. Electrochem. 3 (1987) 11.
[41] A.S. Mogoda, M.M. Hefny, G.A. El Mahdy, Corros. Sci. 46 (1990) 210.
[42] D.J. Blackwood, R. Greef, L.M. Peter, Electrochim. Acta 34 (1989) 875.
[43] Y.Z. Huang, D.J. Blackwood, Electrochim. Acta 51 (2005) 1099.
[44] V. Brunetti, M. López Teijelo, J. Electroanal. Chem. 613 (2008) 16.
[45] L. Young, Anodic Oxide Films, Academic Press, New York, 1962.
[46] M.S. El-Basiouny, S.A. Hassan, M.M. Hefny, Corros. Sci. 20 (1980) 909.
[47] W. Stumm, B. Sulzberger, J. Croat. Chem. Acta 3 (1990) 277.
[48] W. Stumm, in: Chemistry of Solid–Water Interface, Wiley Interscience, New York, 1992, p. 157.
[49] E. Wieland, B. Wehrli, W. Stumm, Geochim. Cosmochim. Acta 52 (1988) 1969.
[50] M.J. Avena, C.P. De Pauli, Colloids Surf. 108 (1996) 181.